A highly potent and selective farnesyltransferase inhibitor ABT-100 in preclinical studies

Wen-Zhen Gu, Ingrid Joseph, Yi-Chun Wang, David Frost, Gerard M. Sullivan, Le Wang, Nan-Horng Lin, Jerry Cohen, Vincent S. Stoll, Clarissa G. Jakob, Steven W. Muchmore, John E. Harlan, Tom Holzman, Karl A. Walten, Uri S. Ladror, Mark G. Anderson, Paul Kroeger, Luis E. Rodriguez, Kenneth P. Jarvis, Debra Ferguson, Kennan Marsh, Shichung Ng, Saul H. Rosenberg, Hing L. Sham and Haiying Zhang

Ras mutation has been detected in approximately 20–30% of all human carcinomas, primarily in pancreatic, colorectal, lung and bladder carcinomas. The indirect inhibition of Ras activity by inhibiting farnesyltransferase (FTase) function is one therapeutic intervention to control tumor growth. Here we report the preclinical anti-tumor activity of our most advanced FTase inhibitor (FTI), ABT-100, and a direct comparison with the current clinical candidates. ABT-100 is a highly selective, potent and orally bioavailable FTI. It broadly inhibits the growth of solid tumors in preclinical animal models. Thus, ABT-100 is an attractive candidate for further clinical evaluation. In addition, our results provide plausible insights to explain the impressive potency and selectivity of ABT-100. Finally, we have demonstrated that ABT-100 significantly suppresses the expression of vascular endothelial growth factor (VEGF) mRNA and secretion of VEGF protein, as well as inhibiting angiogenesis in the animal model. *Anti-Cancer Drugs* 16:1059–1069 © 2005 Lippincott Williams & Wilkins.

Anti-Cancer Drugs 2005, **16**:1059–1069

Keywords: angiogenesis, animal model, crystal structure, farnesyltransferase inhibitor, Ras

Cancer Research, Global Pharmaceutical Research and Development, Abbott Laboratories, Abbott Park, Illinois, USA.

Correspondence to H. Zhang, Cancer Research, Global Pharmaceutical Research and Development, Abbott Laboratories, Abbott Park, Illinois 60064, USA.
Tel: +1 847 938-4857; fax: +1 847 935-7551;
e-mail: haiying.zhang@abbott.com

Received 18 July 2005 **Accepted** 30 July 2005

Introduction

Ras is one of the most frequently mutated genes in human cancers. Oncogenic *ras* is prevalent in pancreatic, colorectal, lung and bladder cancer, and has been detected in approximately 20–30% of all human carcinomas. As such, Ras has been an attractive pharmaceutical target for therapeutic intervention for the past two decades, which includes antisense oligonucleotides, and blocking the formation of activated GTPase and the indirect inhibition of Ras activity by inhibiting farnesyltransferase (FTase) function. FTase is a key enzyme involved in the post-translational modifications required for the attachment of Ras to the plasma membrane, which is critical for Ras signal transduction and biological activity.

FTase is one of three distinct protein prenyltransferases that have been identified in mammalian cells. This cytosolic enzyme is a normal housekeeping protein that transfers a 15-carbon farnesyl group to the cysteine side-chain on the C-terminus of the Ras protein. The other two enzymes transfer the 20-carbon geranylgeranyl group and are referred to as geranylgeranyltransferases I and II (GGTase I and II) [1]. Both FTase and GGTase I are heterodimeric proteins (molecular weight around 94 kDa) that are composed of common α subunits, but distinct, albeit ancestrally related, β subunits. In addition, FTase and GGTase I have similar protein substrate requirements – the so-called C-terminal CAAX motif [2]. These amino acid preferences are not absolute since, in the case of Ras protein substrates, both K-Ras and N-Ras can be prenylated (C-20) by GGTase I when cells are treated with a FTase inhibitor (FTI), which may provide a mechanism to escape the signal blockade [3]. Since only 0.5% of all proteins are farnesylated and 80–90% of these undergo geranylgeranylation, it is desirable to develop FTIs that are highly selective over the closely related enzyme GGTase I in order to avoid interference with critical cellular processes.

However, emerging evidence suggests that the mechanism of action for FTI is not as simple as originally envisioned and Ras is probably neither the only nor the most important farnesylated protein inhibited by FTI for its anti-tumor activity. For example, it has been reported that *ras* mutational status did not correlate with FTI

0959-4973

sensitivity or resistance [4]. Various other targets of FTI had been suggested, such as RhoB – a small GTPase protein that functions in receptor trafficking, cell adhesion and cytoskeletal regulation. RhoB has been proposed to be the relevant downstream target for FTI that causes cell-cycle arrest, apoptosis and tumor regression [5]. Another indirect target of FTI is vascular endothelial growth factor (VEGF) – a specific mitogen for vascular endothelial cells and a pro-survival factor for tumor cells. VEGF is expressed by the vast majority of cancer cells, often at elevated levels. Blocking its activity leads to inhibition of angiogenesis and suppression of tumor growth [6]. It has been shown by us and others that FTI can downregulate the expression of VEGF and inhibit tumor angiogenesis/growth [7].

There are three FTIs (R115777, SCH66336 and BMS214662) undergoing clinical evaluation [8–10]. To date, activity has been observed in patients with leukemia and breast cancer. For example, R115777 displayed a 29% response rate in patients with acute and chronic myeloid leukemia, and a 10% partial response rate in advanced breast cancer [8]. However, two phase III trials of R115777 in pancreatic and colorectal cancer did not demonstrate a significant difference in overall survival [11].

Here, we report the preclinical anti-tumor activity of our most advanced FTI. ABT-100 is a highly selective, potent and orally bioavailable. It broadly inhibits the growth of solid tumors in preclinical animal models. Moreover, the X-ray crystal structures of the complexes between FTase and ABT-100 provide plausible insights for the impressive potency and selectivity of ABT-100. Finally, ABT-100 inhibits the expression of VEGF mRNA and secretion of VEGF protein in cancer cell lines. The anti-angiogenic activity of ABT-100 was further observed in the mouse corneal model.

Materials and methods

Cell lines and chemical compounds

Human colon carcinoma HCT-116 cells (ATCC, Rockville, Maryland, USA) and H-Ras-transformed NIH 3T3 cells, graciously provided by Dr Channing Der (University of North Carolina, USA), were cultured in DMEM.

Human colon carcinoma cells HCT-15 and DLD-1 cells (ATCC), and human lung carcinoma NCI H-460 cells (National Cancer Institute) were cultured in RPMI 1640 medium. All cell lines were supplemented with 10% FBS and 1% antibiotic/antimycotic (Gibco, Grand Island, New York, USA), and cultured at 37°C in a humidified chamber containing 95% air and 5% CO_2. ABT-100, 6-((2*S*)-2-(4-cyanophenyl)-2-hydroxy-2-(1-methyl-1H-imidazol-5-yl)ethoxy)-4′-(trifluoromethoxy)-1,1′-biphenyl-3-carbonitrile, was synthesized by Abbott (Abbott Park, Illinois, USA). The absolute stereochemistry of ABT-100 was determined by X-ray crystal structure. R115777, SCH66336 (racemic compound) and BMS214662 compounds were also synthesized by Abbott.

Crystal structure analysis

Protein for the rat FTase was purified and crystallized in the presence of 2HFP and Ac-CVIM peptide according to the methods outlined in Strickland *et al.* [12]. Crystals of FTase were soaked in a solution containing 0.1 M KCl/0.1 M sodium acetate, pH 4.7 saturated with ABT-100, SCH66336 or R115777 for 24 h at 4°C and flash frozen in the same solution containing 25% glycerol. Data were collected using the synchrotron radiation source at the IMCA 17-ID beamline at Advanced Photon Source (Argon National Laboratory, Darien, Illinois, USA). Data were reduced using the HKL 2000 package [13]. The model 1FT2 from the Brookhaven PDB was used for initial phasing and the structure was refined using CNX [14,15] with a combination of simulated annealing maximum likelihood refinement and either group B-factor refinement (for SCH66336 and R1157777 both to 2.4 Å resolution) or individual B-factor refinement (ABT-100 to 2.4 Å resolution). Electron density maps were inspected on a Silicon Graphics INDIGO2 workstation using the program package QUANTA 97 (Molecular Simulations, San Diego, California, USA)

In vitro enzyme assays

Both FTase and GGTase I inhibitory activity of ABT-100 *in vitro* were determined by scintillation proximity assay (SPA) technology [16]. Briefly, the assay was performed with recombinant human FTase from bacculovirus and purified bovine brain FTase or GGTase, [^{3}H]FPP (NEN, Boston, Massachusetts, USA) and a biotin-conjugated K-Ras (B) decapeptide (KKSKTKCVIM) or pentapeptide (GCVLL) in 50 mM HEPES, 30 mmol/l $MgCl_2$, 20 mmol/l KCl, 5 mM DDT and 0.01% Triton X-100, pH 7.0. After a 30-min incubation, stop/streptandin-coated bead reagent was added and the counts associated with the beads were determined using a Packard TopCount scintillation plate reader (Packard, Meriden, Connecticut, USA).

Ras and Rap 1A processing assay

Western blot assay was performed to determine the potency of FTIs in blocking Ras or Rap 1A post-translational processing in intact cells. The processed and unprocessed Ras or Rap 1A were separated by 15% Tris–glycine gel (Bio-Rad, Hercules, California, USA), immunoblotted with a pan-Ras antibody or Rap 1A antibody (Transduction, Lexington, Kentucky, USA) and quantified by densitometry using the image analysis program Image-Pro Plus (Media Cybernetics, Silver Spring, Maryland, USA).

Fig. 1

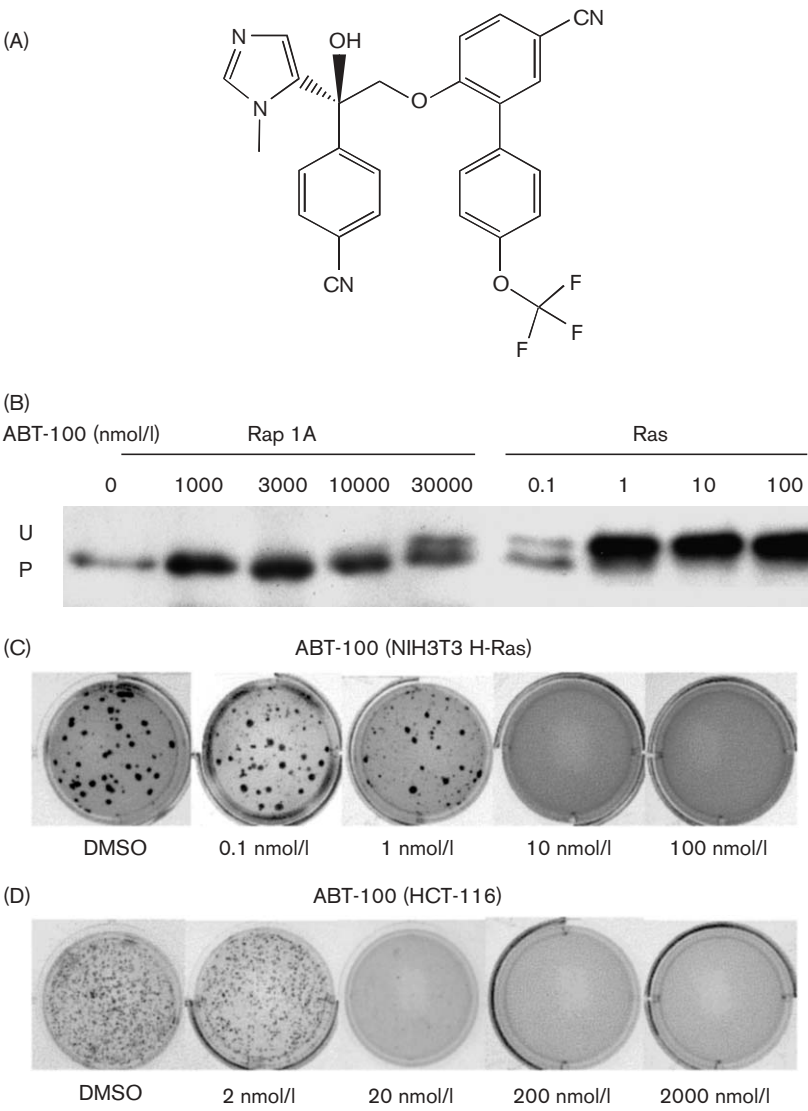

(A) Chemical structure of ABT-100. (B) Effects of increasing concentrations of ABT-100 on the processing of Ras protein and Rap 1A protein in H-Ras-transformed murine NIH 3T3 cells, respectively. The lower and upper bands represent processed (P) and unprocessed (U) protein, respectively. (C) The effect of ABT-100 on the anchorage-independent growth in H-ras-transformed murine NIH 3T3 cells. Approximately 5×10^3 NIH 3T3 H-Ras cells were inoculated into each well of 12-well culture plates on a 0.35% top agar layer overlaid with 0.7% agar with ABT-100 with 10% FBS. After 14 days of incubation, colonies from triplicate wells were photographed using a Sony CCD camera and quantified by Image-Pro Plus software. (D) The effect of ABT-100 on the anchorage-independent growth in human colon carcinoma HCT-116 cells. Conditions are described in Materials and methods.

Quantitative RT-PCR analysis for VEGF mRNA

HCT-116 cells were seeded in 100-mm dishes (Corning, New York, New York, USA) at a density of 40–50% confluence overnight and then cells were treated with various concentrations of ABT-100 or 0.1% DMSO for an additional 3 days. RNA isolation was performed using a Qiagen (Valencia, California, USA) RNeasy mini-kit according to the manufacturer's instruction. The relative levels of VEGF (VEGF A) were assessed by quantitative RT-PCR (TaqMan) technology. All TaqMan probes were

Table 1 ***In vitro*** **potency of ABT-100 and other FTIs**

Compound	IC_{50}(nmol/l)[a]		
	Bovine Ftase	Human Ftase	Bovine GGTase I
ABT-100	0.13 ± 0.01 (n=4)	0.05 ± 0.01 (n=6)	>10000 (n=3)
R115777[b]	0.57 ± 0.06 (n=3)	0.45 ± 0.08 (n=3)	1043 ± 57 (n=3)
SCH66336[c]	7.8 ± 1.6 (n=3)	4.9 ± 1.1 (n=3)	>10,000 (n=3)
BMS214662[d]	0.67 ± 0.06 (n=3)	0.21 ± 0.02 (n=3)	990 ± 110 (n=3)

[a]Mean ± SEM.
[b]Janssen.
[c]Schering-Plough.
[d]Bristol-Myers Squibb.

5′-labeled with the reporter fluorescein and 3′-labeled with the quencher tetramethylrhodamine. The VEGF A sequences for forward and reverse primers were 5′-TACCTCCACCATGCCAAGTG-3′ and 5′-GATGATTCT GCCCTCCTCCTT-3′, respectively. The TaqMan probe used was 5′-[FAM]TCCCAGGCTGCACCCATGGC [TAMRA]-3′. The 28S rRNA sequences for forward and reverse primers were 5′-TTCACCAAGCGTTG-GATTGTT-3′ and 5′-TGTCTGAACCTGCGGTTCCT-3′, respectively, and the TaqMan probe used was 5′-[HEX]TCACGACGGTCTAAACCCAGCTCACG[TAM-RA]-3′. Samples for quantitative RT-PCR analysis were 100 ng of total RNA. Each quantitative RT-PCR reaction was prepared in triplicate in a final volume of 25 µl. Data was collected during each extension phase of the PCR reaction and analyzed with the ABI-7700 SDS software package. Threshold cycles were determined for each gene. A parallel standard curve (in duplicate) was generated for the VEGF gene and the 28S rRNA. This standard curve was used to determine the relative concentration of RNA in each sample by comparison using methods described in *PE-ABI Prism 7700 Users Bulletin Number 2*. The expression values were normalized to the untreated control and are shown ± SD.

VEGF secretion

HCT-116 or NCI H-460 cells were plated at a density of 25 000 cells/well of a 24-well plate. Cells were treated with DMSO or various concentrations of ABT-100 for 3 days. Conditioned medium was harvested and determined for levels of VEGF secretion using an ELISA kit according to manufacturer's instruction (R & D Systems, Minneapolis, Minnesota, USA). The level of VEGF secretion was normalized against total cell counts in each well.

Table 2 Cellular potency of ABT-100 and other FTIs in Ras and Rap 1A processing assays in Ras transformed murine fibroblast cells

Compound	EC_{50}(nmol/l)[a]	
	NIH 3T3 H-Ras with 10% bovine serum (nmol/l)	NIH 3T3 H-Ras with 10% bovine serum Rap 1A (µmol/l)
ABT-100	0.73 ± 0.09	>30
R115777[b]	2.3 ± 0.6	>30
SCH66336[c]	160 ± 16	>30
BMS214662[d]	84 ± 8	>30

[a]Mean (n = 3) ± SEM.
[b]Janssen.
[c]Schering-Plough.
[d]Bristol-Myers Squibb.

Soft agar colony formation assay

For anchorage-independent growth, 5000 NIH 3T3 H-Ras or HCT-116 cells were inoculated onto each well of 12-well culture plates on a 0.35% top agar layer overlaid with 0.7% agar with the same medium supplemented with 10% FBS. Both agar layers contained ABT-100 at various doses. Cultures were re-fed with compound or vehicle twice a week. After 14 days of incubation, colonies from triplicate wells were photographed using a Sony CCD camera and quantified by Image-Pro Plus. Assay results were expressed by percent inhibition relative to vehicle controls.

Animal studies

Human tumor xenograft in nude mice

Efficacy of ABT-100 was evaluated against human solid tumors in several mouse flank models including HCT-116 and DLD-1 human colon carcinoma models. Briefly, for HCT-116 and DLD-1 models, male *nu/nu* CD1 mice aged 8 weeks (Charles River, Massachusetts, USA, Maine) were housed in barrier facilities with food and water *ad libitum*. Two million HCT-116 or DLD-1 cells mixed 1:1 with Matrigel in a total volume of 0.2 ml were inoculated s.c. into the mouse flank. In the DLD-1 colon carcinoma model, tumor cells were inoculated 5 days prior to treatment. Mice received ABT-100 at 6.25, 12.5 or 25 mg/kg/day s.c., on a q.d. × 21 days. The tumors were measured by a pair of calipers twice a week after tumors were palpable and the tumor volumes were calculated according to the formula $V = L \times W^2/2$ (V = volume, L = length and W = width). In an established HCT-116 xenograft model, 14 days post-tumor cell inoculation, mice received either vehicle (n = 10) or A-367074, a racemate of ABT-100, at 50 mg/kg/day dose (n = 10), respectively. In an early treatment HCT-116 model, animals were treated with A-367074 at 100 mg/kg/day in a q.2d. regimen 5 days prior tumor inoculation. This q.2d.

Table 3 Cellular potency of ABT-100 and other FTIs in Ras processing assays in human cancer cell lines with varying levels of P-gp expression

Human cancer cell lines	EC_{50}(nmol/l)[a]			
	ABT-100	R115777[b]	SCH66336[c]	BMS214662[d]
HCT-116 with 10% FBS	0.43 ± 0.05	0.98 ± 0.06	16 ± 0.58	12 ± 0.88
HCT-116 with 20% human serum	1.7 ± 0.18	6.7 ± 0.67	49 ± 4.7	23 ± 3.5
DLD-1 with 10% FBS	0.26 ± 0.04	0.69 ± 0.01	12 ± 0.33	9.4 ± 0.81
DLD-1 with 20% human serum	0.40 ± 0.23	3.1 ± 1.0	23 ± 4.1	12 ± 2.1
HCT-15 with 10% FBS	0.20 ± 0.04	0.55 ± 0.07	37 ± 7.0	39 ± 3.0
HCT-15 with 20% human serum	1.1 ± 0.09	4.9 ± 0.30	210 ± 15	98 ± 0.90

[a]Mean (n = 3) ± SEM
[b]Janssen.
[c]Schering-Plough.
[d]Bristol-Myers Squibb.

treatment schedule was compare to Janssen's compounds given daily on a b.i.d. schedule.

Mouse corneal angiogenesis model

The anti-angiogenic activity *in vivo* was determined using the corneal model in female CF1 mice (Charles River). Briefly, a uniformed shape and size hydron-sucralfate pellet from a pellet maker containing either 30 ng of human recombinant basic fibroblast growth factor (bFGF; Collaborative Research, Bedford, Massachusetts, USA) or 150 ng human recombinant VEGF (Collaborative Research) was inserted in corneal pocket of the right and left cornea, respectively. Mice were administered ABT-100 at 25, 50 and 100 mg/kg/day were s.c. treated on a once-a-day treatment. On day 5 (bFGF) and day 7 (VEGF), a corneal image was obtained by using a digital camera attached to a slit lamp biomicroscope (NS-1; Nikon, Tokyo, Japan). The neovascular measurement field was the area and length between the pellet and the limbus where neovascularization had occurred. Data acquisition and storage were achieved with Leica imaging software (Qwin; Leica, Cambridge, UK). The statistical significance was evaluated with a two-tailed *t*-test. Neovascularization from animals receiving drug was expressed as a percent of untreated controls ± SD.

Table 4 Cellular potency of ABT-100 and other FTIs in soft agar colony formation assay

Compound	EC_{50}(nmol/l)[a]	
	NIH 3T3 H-Ras with 10% bovine serum (nmol/l)	HCT-116 with 10% FBS (nmol/l)
ABT-100	0.90	6.1
R115777[b]	3.7	24
SCH66336[c]	56 (50)[e]	94 (74)[e]
BMS214662[d]	79 (25)[e]	170

[a]Mean ± SEM.
[b]Janssen.
[c]Schering-Plough.
[d]Bristol-Myers Squibb.
[e]EC_{50} from Schering-Plough or Bristol-Myers Squibb.

Table 5 The pharmacokinetic profile of ABT-100 in rat and dog

	Dose i.v.					Dose p.o.				
	Dose (mg/kg)	$t_{1/2}$(h)	$V_{\hat{a}}$(l/kg)	AUC (μg·h/ml)	CL_p(l/h/kg)	Dose	$t_{1/2}$(h)	C_{max} (μg/ml)	AUC (μg·h/ml)	*F* (%)
Rat	5	2.3	5.6	3.01	1.2	5	NC	0.08	0.45	15.1
						25	NC	0.74	4.62	30.7
Dog	2.5	6.8	3.3	7.7	0.34	2.5	5.9	0.28	2.84	35.1

NC: unable to calculate.

Fig. 2

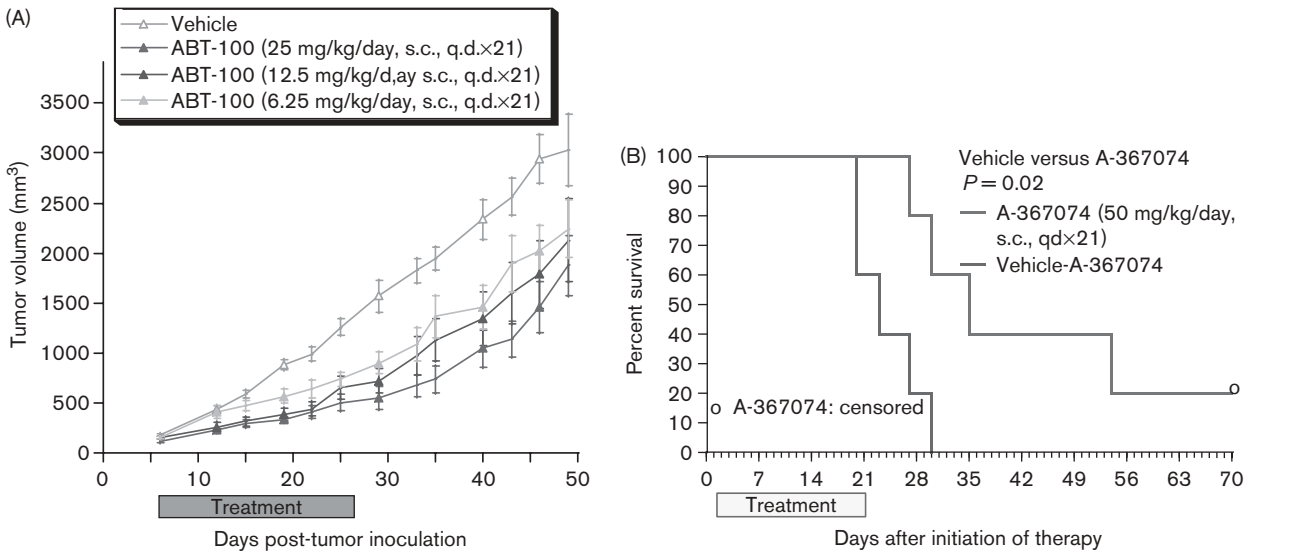

(A) The effect of ABT-100 on the growth of DLD-1 colon carcinoma in nude mice ($N = 10$/group). Tumor cells were inoculated 5 days prior to treatment. Mice received ABT-100 at 6.25, 12.5 and 25 mg/kg/day s.c., q.d. × 21 days. The first day of therapy was designated as day 1. (B) Effect of A-367074 (racemate of ABT-100) on survival time of HCT-116 tumor-bearing nude mice ($N = 5$/group). Tumor cells were inoculated 14 days prior to treatment. Animals were size-matched for established tumors (350 mm^3). Mice received A-367074 at 50 mg/kg/day s.c., q.d. × 21 days. The first day of therapy was designated as day 1.

Table 6 Dose-dependent efficacy of ABT-100 in the DLD-1 early treatment xenograft model (therapy was initiated 5 days post-tumor cell inoculation)

Compound	Dose (mg/kg/day)	Route/schedule	Tumor volume (day 25)[a]	%T/C[b](day 25)	%ILS[c]
ABT-100	25	s.c., q.d. × 21	553 ± 113	32[***d]	100[***]
	12.5		721 ± 125	39[***]	61[***]
	6.25		899 ± 111	56[*]	50[**]
Vehicle		s.c., q.d. × 21	1569 ± 165		

[a]Mean (mm3) ± SEM.
[b]Ratio of tumor volume for treated versus control (vehicle), calculated from log-transformed data.
[c]Median percent increase compared to vehicle in time to 1 cm^3 tumor calculated considering the first day of treatment as day 1.
[d]Significance: $^{*}P<0.05$, $^{**}P<0.01$ and $^{***}P<0.001$ versus vehicle.

Table 7 Efficacy of A-367074 (racemate of ABT-100) in an established HCT-116 xenograft model [animals were size-matched for established tumors (350 mm^3) and therapy initiated 14 days post-tumor cell inoculation]

Compound	Dose (mg/kg/day)	Route/schedule	Tumor volume (day 40)[a]	%T/C[b](day 40)	%ILS[c]
A-367074	50	s.c., q.d. × 21	1530 ± 465	45[* d]	52[*]
Vehicle/A-367074			2913 ± 593		
Camptosar	50	i.p., q.4d. × 4	635 ± 122	22[***]	200[**]
Vehicle/camptosar			2932 ± 636		

[a]Mean (mm3) ± SEM.
[b]Ratio of tumor volume for treated versus control (vehicle), calculated from log-transformed data.
[c]Median percent increase compared to vehicle in time to 1 cm^3 tumor calculated considering the first day of treatment as day 1.
[d]Significance: $^{*}P<0.05$, $^{**}P<0.01$ and $^{***}P<0.001$ versus vehicle.

Table 8 Dose-dependent efficacy of A-367074 in an HCT-116 early treatment xenograft model (therapy was initiated 5 days post-tumor cell inoculation)

Compound	Dose (mg/kg/day)	Route/schedule	Tumor volume (day 22)[a]	%T/C[b](day 22)	%ILS[c]
A-367074	100[e]	s.c., q.2d. × 11	691 ± 75	51[**d]	32[*]
	50		873 ± 89	65	32
Vehicle/A-367074		s.c., q2d × 11	1557 ± 370		
R115777	100	s.c., b.i.d. × 21	820 ± 168	56[*]	39[*]
Vehicle/R115777		s.c., b.i.d. × 21	1436 ± 263		
Gemcitabine	30	i.p., q.3d. × 4	359 ± 21	22[***]	112[***]
Vehicle/gemcitabine			1861 ± 410		

[a]Mean (mm3) ± SEM.
[b]Ratio of tumor volume for treated versus control (vehicle), calculated from log-transformed data.
[c]Median percent increase compared to vehicle in time to 1 cm^3 tumor calculated considering the first day of treatment as day 1.
[d]Significance: $^{*}P<0.05$, $^{**}P<0.01$ and $^{***}P<0.001$ versus vehicle.
[e]MTD.

Results

In vitro potency and selectivity of ABT-100

ABT-100 (Fig. 1A) is potent and highly selective *in vitro*, as well as at the cellular level. It inhibits bovine and human FTase with IC_{50} values of 0.13 and 0.05 nmol/l, respectively, and is more than 100 000-fold selective for FTase over the closely related enzyme GGTase I (Table 1). To demonstrate that the compound is selective for its relevant enzyme targets in cells, we used an immunoblot method to monitor prenylation inhibition of Ras and Rap 1A for measuring the activity of FTase and GGTase I, respectively. The concentration at which prenylation was inhibited by 50% was assigned as the EC_{50} value. ABT-100 potently and selectively inhibited FTase in cells with an EC_{50} value of 0.73 nmol/l in Ras processing. The EC_{50} values in the same assay for R115777, SCH66336 and BMS214662 were 2.3, 160 and 84 nmol/l, respectively. The selectivity assay was performed with an exclusively GGTase I substrate, Rap 1A. The EC_{50} value was above 30 μmol/l (Fig. 1B). ABT-100 showed more than 41 000-fold selectivity for Ras over Rap 1A (Table 2).

In order to determine the effect of human serum protein binding and to ascertain whether ABT-100 is a substrate for the P-glycoprotein efflux pump (P-gp-1), the cellular potencies of these compounds were determined in the presence of 20% human serum in three human cancer cell lines with different levels of P-gp-1 expression: HCT-15 (high), DLD-1 (moderate) and HCT-116 (low) [17]. As summarized in Table 3, the potency of ABT-100 is not affected by the level of P-gp-1 expression in the cells as it showed similar EC_{50} values in HCT-15 and HCT-116 cells, which have relatively high and low levels of P-gp-1, respectively. Thus, the results indicate that ABT-100 is not a substrate of P-gp-1. In addition, only minimal loss of cellular potency was observed for ABT-100 in the presence of 20% human serum (1.5- to 5.6-fold loss of

Fig. 3

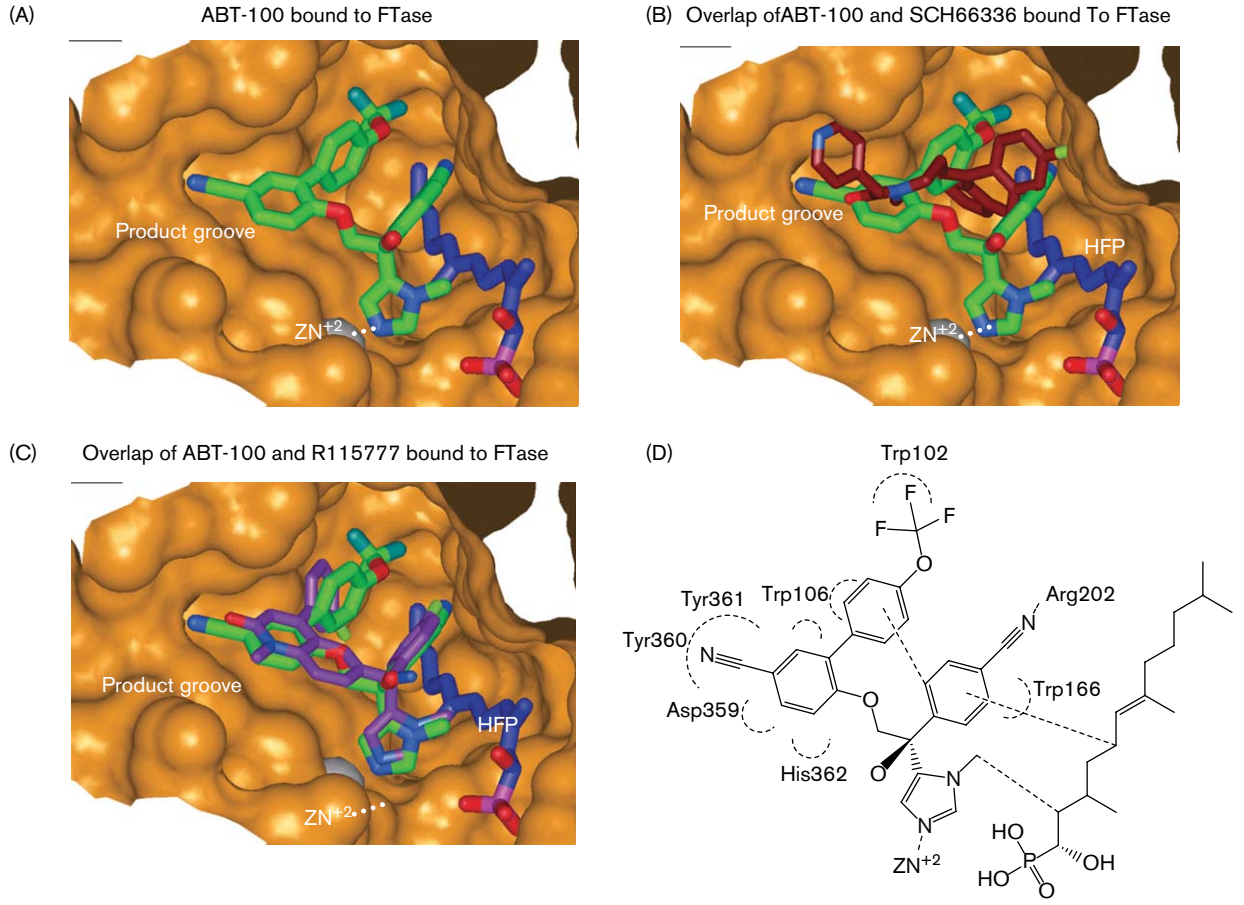

(A) The X-ray crystal structure of FTase complexed with ABT-100 (green), HFP (blue) and Zn^{2+} (grey) at 2.4 Å resolution with R_{work} = 25.98% and R_{free} = 29.14%. (B) The overlap of X-ray crystal structure of FTase complexed with ABT-100 (green), HFP (blue), Zn^{2+} (grey) and SCH66336 (brown) at 3.5 Å resolution with R_{work} = 25.39% and R_{free} = 35.03%). (C) The overlap of X-ray crystal structure of FTase complexed with ABT-100 (green), HFP (blue), Zn^{2+} (grey) and R115777 (purple) at 3.5 Å resolution with R_{work} = 23.61% and R_{free} = 30.17%. (D) Schematic diagram of the binding mode of ABT-100 in the active site of FTase.

potency in the three cell lines tested). R115777 is also not a substrate of P-gp-1 and its cellular potency is not affected significantly by the addition of 20% human serum (4.4- to 8.9-fold loss). SCH66336 and BMS214662 are weak substrates of P-gp-1, consistent with the reported data [18]. A minimal loss of cellular activity (1.9- to 5.7- and 1.3- to 2.5-fold, respectively) was observed for these two compounds in the presence of 20% human serum.

Inhibition of anchorage-independent cell growth

The soft agar colony formation assay was used to ascertain the potency of ABT-100 in the inhibition of the anchorage-independent growth of cells. ABT-100 showed a dose-dependent reduction of colony formation (Fig. 1C and D) with EC_{50} values of 0.9 and 6.1 nmol/l for H-Ras-transformed NIH 3T3 and HCT-116 human colon carcinoma cells with the K-Ras mutation, respectively. The EC_{50} values for R115777, SCH66336 and BMS214662 were 3.7, 56 and 79 nmol/l in H-Ras-transformed NIH 3T3 cells, and 24, 94 and 170 nmol/l in HCT-116 cells, respectively (Table 4).

Pharmacokinetics profile of ABT-100

The ABT-100 plasma clearance value following i.v. dosing in the rat is 1.0-1.2 l/h·kg. It is characterized by high volumes of distribution ($V > 2$ l/kg), with elimination half-lifes above 1.5 h. The bioavailability value for ABT-100 in rat is 15.1%. Table 5 summarizes the pharmacokinetics of ABT-100 in rat and dog. We observed similar trends in monkey (unpublished data) and a better pharmacokinetics profile in mice.

In vivo anti-tumor activity

Two colon cancer cell lines, DLD-1 and HCT-116, were evaluated in the xenograft models. The DLD-1 xenograft

Fig. 4

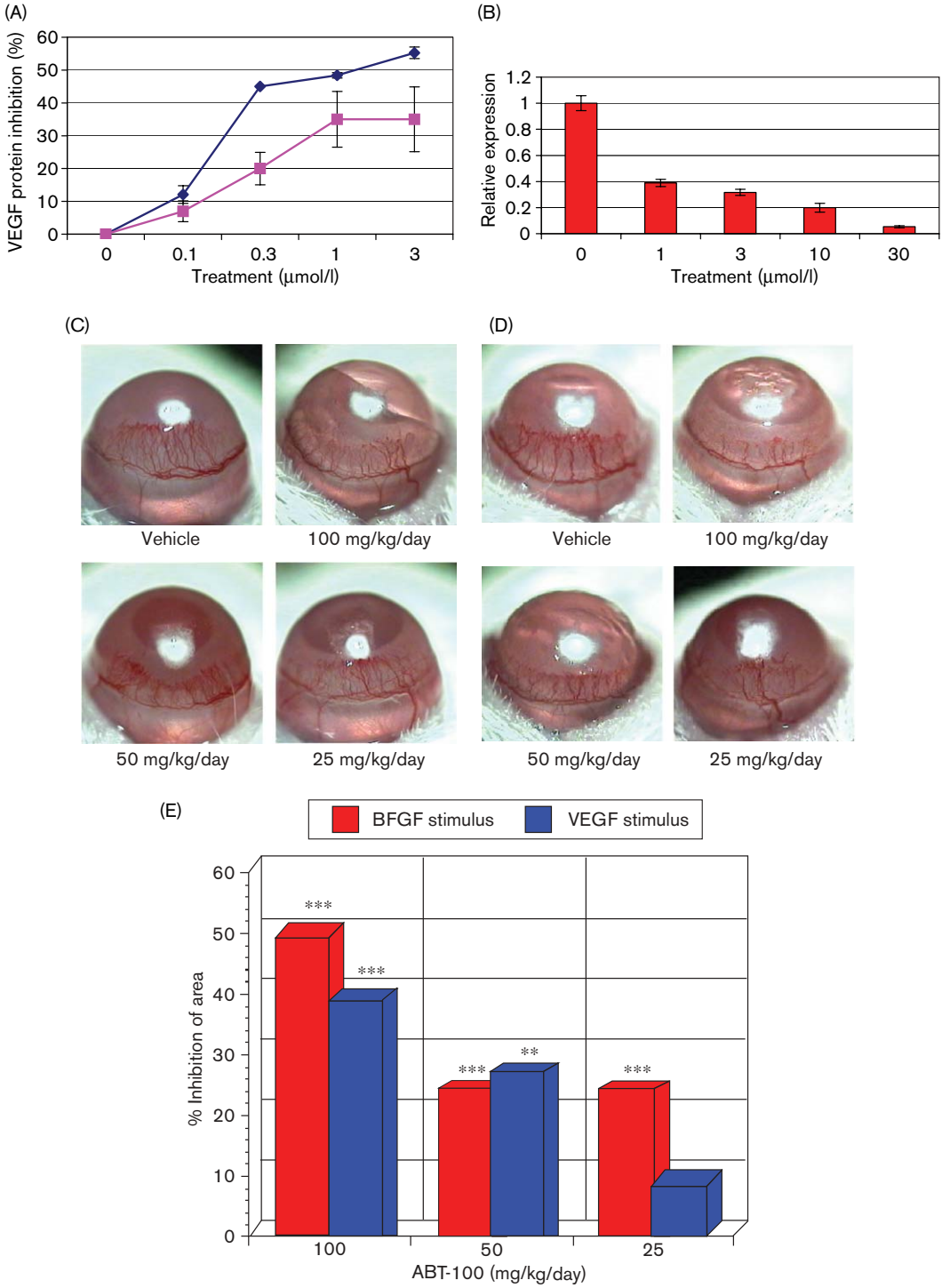

(A) ABT-100 inhibited secretion of VEGF protein in HCT-116 (diamonds) and NCI H-460 (squares). Both cells were seeded into 24-well plates at a density of 5000 cells/well and incubated with increasing ABT-100 doses. The supernatant was collected after 72 h of treatment for the detection of VEGF protein using ELISA. (B) VEGF mRNA expression in HCT-116 cells. HCT-116 cells were seeded into 100-mm dishes at 40–50% confluency for 24 h. Cells were treated with various concentrations of ABT-100 for 72 h, and RNA was isolated and evaluated with quantitative RT-PCR. VEGF gene expression values were determined from a standard curve, then normalized to control 28S rRNA amplification. (C, D and E) Anti-angiogenic activity of ABT-100 in the mouse corneal model. CF1 mice received ABT-100 at 25, 50 and 100 mg/kg/day s.c., q.d. for 7 days. Treatment was initiated immediately after growth factor pellet implant (30 ng bFGF, 150 ng VEGF). Vessel formation was evaluated at Day 7 for VEGF-induction (C) and Day 5 for bFGF-induction (D). Historically, the maximum inhibition with antiangiogenic agents is 50–60% in this model. The bars with asterisks (*) indicate statistical difference from vehicle control (E). $p<0.01$**, $p<0.001$***.

grows rapidly in nude mice, reaching 1 cm^3 tumor volume in 19–24 days, while the HCT-116 xenograft reaches the same size in untreated animals in 26–29 days. ABT-100 demonstrated highly significant efficacy in the DLD-1 early treatment model as reflected by both the T/C values of 32, 39 and 56%, and ILS values of 100, 61 and 50% at doses of 25, 12.5 and 6.25 mg/kg/day, respectively (Fig. 2A and Table 6 and 7). Further, the HCT-116 established tumor model was used to evaluate efficacy of A-367074, the racemate of ABT-100. The EC_{50} values against FTase *in vitro* and at the cellular level were 0.6 and 2 nmol/l, respectively. Although A-367074 is 4.6- and 2.7-fold less potent than ABT-100 in both cellular assays, it displayed good efficacy in this animal model with a T/C value of 45% tested at 50 mg/kg/day dose given on a q.d. schedule (Table 6). Kaplan–Meier survival curves demonstrate that A-367074 significantly improved median survival duration by 52% (Fig. 2B). Subsequently, we used the HCT-116 early treatment model to compare the efficacy of A-367074 with R115777. A-367074 demonstrated good efficacy in the HCT-116 early treatment model at 100 mg/kg/day given on a q2d schedule. R115777 (%T/C = 56) displayed a comparable efficacy with A-367074 (%T/C = 51) (Table 8). However, it is worth to note that A-367074 was dosed less frequently and for shorter time than R115777 (q2d × 11 versus b.i.d. × 21 days).

Crystal structure of ABT-100 and binding mode

The X-ray crystal structure of FTase complexed with hydroxy farnesyl phosphate (HFP) and ABT-100 has been determined to 2.4 Å resolution (Fig. 3A). The crystal structure reveals that HFP forms part of the binding site for ABT-100 as has been observed for SCH66336, R1155777 (Fig. 3B–D) and the peptide substrate with the first phenyl ring stacking over Tyr361, Asp359 and His362. The *para*-cyano group on the biphenyl is directly over the protein backbone loop of residues Tyr361, Tyr360 and Asp359 (Fig. 3D). From the top and sides, this cyanobiphenyl is in van der Waals contact with Trp106, Leu96 and Tyr93. The trifluoromethoxy group of the biphenyl binds deep in the peptide substrate site and makes close van der Waals or stacking interactions with Tyr361 and Trp106, while the *para*-trifluoromethyl ether interacts directly with Trp102. It is important to note that the compound is further stabilized in the binding site by the hydrophobic collapse of the cyanobiphenyl-–trifluoromethoxy stacking with the cyanophenyl group that is bound next to HFP. Finally, additional binding interactions involve the methyl histidine electrostatically binding to the Zn^{2+}. The cyanophenyl moiety of ABT-100 lies across the HFP alkyl chain and makes additional van der Waals contact with Tyr166 with the *para*-cyano group hydrogen bonded to Arg202. The second cyano group on the biphenyl ring occupies a portion of the product-binding pocket proposed by Long *et al.* [19].

ABT-100 inhibits VEGF expression and secretion

In order to evaluate whether the effect of anti-tumor activity exhibited by ABT-100 is concomitantly through anti-angiogenesis, we have examined the effect of ABT-100 on the transcription and secretion of VEGF – a key mitogen for vascular endothelial cells. The results from quantitative RT-PCR analysis indicated that ABT-100 inhibited VEGF mRNA expression in a dose-dependent manner (Fig. 4B). Correspondingly, the secretion of VEGF protein from human tumor cells was inhibited by ABT-100 in a dose-dependent manner as measured by ELISA assays (Fig. 4A). It was also confirmed that ABT-100 decreased the VEGF level in tumor tissue (data not shown).

The efficacy of ABT-100 in angiogenesis models *in vivo*

To extend the observation of the ABT-100 inhibitory effect on the expression and secretion of VEGF, the murine corneal model was used to evaluate the anti-angiogenesis potential of ABT-100. Implantation of either bFGF or VEGF causes a florid growth of blood vessels within the avascular cornea of untreated mice. The neovascularization of the cornea was then quantified by image analysis after 7 (for VEGF) or 5 days (for bFGF), respectively. The experimental results showed that ABT-100 at 25, 50 and 100 mg/kg/day inhibited the growth of new blood vessel area by 8, 25 and 39% following stimulation with VEGF or 23, 24 and 49% with bFGF, respectively (Fig. 4C and D). The results indicate that ABT-100 has anti-angiogenesis activity, which is independent of its activity of inhibiting VEGF production.

Discussion

In the present study, we have shown that ABT-100 is a potent and highly selective (more than 100 000-fold) FTI. In addition, ABT-100 possesses an excellent cellular potency in human tumor cells (Table 3). The cellular activity of ABT-100 is not significantly affected by the presence of human serum or the expression of the PgP-1 drug efflux pump. The cellular potency of ABT-100 has been further demonstrated in the inhibition of the anchorage-independent growth of H-Ras-transformed murine and human cancer cell lines with EC_{50} values of 0.9 and 6.1 nmol/l, respectively (Table 4).

Moreover, the results from xenograft models have validated the potency of ABT-100 *in vivo*. It achieves 49–55 and 68% inhibition of tumor growth with human colon cancer cells HCT-116 and DLD-1, respectively. ABT-100 showed good efficacy in additional xenograft models as well (data not shown). R115777, the most advanced FTI in clinical development, was chosen for comparison to the *in vivo* potency with ABT-100. ABT-100 displayed a comparable or better efficacy compared with R115777 since the mice were treated with ABT-100 q2d for 11 days and R115777 did for 21 days. It will be

interesting to know whether longer exposure of ABT-100 will further improve the efficacy.

We believe that the excellent efficacy of ABT-100 is the result of its high intrinsic potency and its optimal pharmacokinetic profile, which ensure sufficient exposure and inhibition of FTase *in vivo*. Peak plasma concentration and values of ABT-100 are 2.18 μg/ml and 27 μg/h·ml, respectively, following 25 mg/kg s.c. qd dosing in nude mice. Oral bioavailability of ABT-100 is 79% in HCT-116 tumor-bearing nude mice, which appears to be better than that in rat or dog, as indicated in Table 4. In addition, the ABT-100 has very low plasma clearance values following i.v. dosing in the dog, with high volumes of distribution and a substantially long apparent elimination half-life. The high volumes of distribution contribute to the comparatively lower peak plasma concentrations, which will ensure relatively constant drug exposure. More importantly, crystallographic studies show that the binding interactions of ABT-100 to FTase, including the strong electrostatic interactions of the methyl imidazole with the active-site Zn^{2+}, and the direct protein and farnesyl pyrophosphate (or HFP) interactions, provide high potency. Without knowing the binding mode of ABT-100 to GGTase, it is not possible to determine exactly why ABT-100 shows such good selectivity for FTase over GGTase; however, we do know that the trifluoromethyl group of ABT-100 interacts with Trp102 (Fig. 3D), which corresponds to a serine residue in GGTase. The loss of this key interaction may cause its low potency against GGTase I and contribute to the excellent selectivity profile of ABT-100.

A large number of studies have shown that *ras* mutations can lead to induction of VEGF expression in a diverse and broad array of experimental systems in both animal and human cell lines [20–22]. VEGF can act as a survival factor for the endothelial cells of newly formed immature blood vessel capillaries [23], by which tumor cells grow and survive. FTIs can block VEGF production *in vitro* and angiogenesis effects *in vivo* [24,25]. Therefore, death of tumor cells could be the result of preventing growth of the new blood vessels and the regression of existing ones [26]. We have demonstrated that ABT-100 strongly inhibited VEGF expression and secretion *in vitro*. Additionally, ABT-100 also demonstrated an anti-angiogenesis effect induced by VEGF and bFGF in the corneal model. The results indicate that the mechanism of the anti-angiogenesis effect of ABT-100 is more than just the inhibition of VEGF production. Thus, ABT-100 is an attractive candidate for further clinical evaluation.

In conclusion, this report has demonstrated that ABT-100 is a highly selective, potent and orally bioavailable FTI, which may be attributable to its unique binding mode to FTase and good pharmacokinetics profile.

Acknowledgements

We gratefully acknowledge technical and material support for SPA FTase assays from Tom Lubben and Jill Clampit. For crystal structure analysis, data were collected at beamline 17-ID in the facilities of the Industrial Macromolecular Crystallography Association Collaborative Access Team (IMCA-CAT) at the Advanced Photon Source. These facilities are supported by the companies of the Industrial Macromolecular Crystallography Association.

References

1 Gibbs J, Oliff A. The potential of farnesyltransferase inhibitors as cancer chemotherapeutics. *Annu Rev Pharmacol Toxicol* 1997; **37**:143–166.
2 Moores SL, Schaber MD, Mosser SD, Rands E, O'Hara MB, Garsky VM, *et al.* Sequence dependence of protein isoprenylation. *J Biol Chem* 1991; **266**:14603–14610.
3 Prendergast GC, Oliff A. Characterization of prenyl groups attached to K-Ras in DLD-1 human colon carcinoma cells treated with the FPT inhibitor SCH 44342. *Proc Am Ass Cancer Res* 1996; **37**:503.
4 Cox AD. Farnesyltransferase inhibitors: potential role in the treatment of cancer. *Drugs* 2001; **61**:723–732.
5 Prendergast GC, Oliff A. Farnesynlation inhibitors: antineoplastic mechanism and clinical prospects. *Semin Cancer Biol* 2000; **10**:443–452.
6 Folkman J. Angiogenesis in cancer, vascular, rheumatoid and other disease. *Nat Med* 1995; **1**:27–31.
7 Rak J, Kerbel RS. Ras regulation of vascular endothelial growth factor and angiogenesis. *Methods Enzymol* 2001; **333**:267–283.
8 Widemann BC, Fox E, Goodspeed W, Goodwin A, Jayaprakash N, Pitney A, *et al.* Phase I trial of the farnesyltransferase inhibitor (FTI) R115777 in children with refractory leukemias. *Proc Am Soc Clin Oncol* 2003; **22**:809.
9 Awada A, Eskens FA, Piccart M, Cutler DL, van der Gaast A, Bleiberg H, *et al.* Phase I and pharmacological study of the oral farnesyltransferase inhibitor SCH 66336 given once daily to patients with advanced solid tumours. *Eur J Cancer,* 2002; **38**:2272–2278.
10 Caponigro F, Casale M, Bryce J. Farnesyl transferase inhibitors in clinical development. *Expert Opin Invest Drugs,* 2003; **12**:943–954.
11 Zhu K, Hamilton A, Sebti S. Farneysltransferase inhibitors as anticancer agent: current status. *Curr Opin Invest Drug* 2003; **21**:1428–1435.
12 Strickland C, Windsor WT, Syto R, Wang L, Bond R, Wu Z, *et al. Biochemistry* 1998; **37**:16601.
13 Otwinowski Z, Minor W. *Methods Enzymol* 1997; **276**:307–326.
14 Brunger AT, Adams PD, Clore GM, Delano WL, Gros P, Grasse-Kunstleve RW, *et al. Biol Crystallogr* 1998; **54**:905.
15 Badger J, Berard D, Kumar RA, Szalma S, Yip P, Griesinger C, *et al. CNX software manual*. San Diego, California: Molecular Simulations; 1999.
16 Tahir SK, Gu WZ, Zhang HC, Leal J, Lee JY, Kovar P, *et al.* Inhibition of farnesyltransferase with A-176120, a novel and potent farnesyl pyrophosphate analogue. *Eur J Cancer* 2000; **36**:1161–1170.
17 http://dtpsearch.ncifcrf.gov/DATA/MOLECULAR_TARGETS/TABLES/RHODVAL.HTML.
18 Wang E, Casciano CN, Clement RP, Johnson WW. The farnesyl protein transferase inhibitor SCH66336 is a potent inhibitor of MDR1 product P-glycoprotein. *Cancer Res* 2001; **61**:7525–7529.
19 Long SB, Casey PJ, Beese LS. Reaction path of protein farnesyltransferase at atomic resolution. *Nature* 2002; **419**:645.
20 Grugel S, Finkenzeller G, Weindel K, Barleon B, Marme D. Both v-Ha-Ras and v-Raf stimulate expression of the vascular endothelial growth factor in NIH 3T3 cells. *J Biol Chem* 1995; **270**:25915–25919.
21 Okada F, Rak JW, Croix BS, Lieubeau B, Koya M, Roncari L, *et al.* mutant K-*ras* up-regulation of vascular endothelial growth factor/vascular permeability factor is necessary, but not sufficient for tumorigenicity of human colorectal carcinoma cells. *Proc Natl Acad Sci USA* 1998; **95**:3609–3614.
22 Larcher F, Robles AI, Duran H, Murillas R, Quintanilla M, Cano A, *et al.* Up-regulation of vascular endothelial growth factor/vascular permeability factor in mouse skin carcinogenesis correlates with malignant progression state and activated H-*ras* expression levels. *Cancer Res* 1996; **56**:5391–5396.
23 Alon T, Hemo I, Itin A, Pe'er J, Stone J, Keshet E. Vascular endothelial growth factor acts as a survival factor for newly formed retinal vessels and has implications for retinopathy of prematurity. *Nat Med* 1995; **1**:1024–1028.

24 Rak J, Mitsuhashi Y, Bayko L, Filmus J, Shirasawa S, Sasazuki T, *et al.* Mutant *ras* oncogenes upregulate VEGF/VPF expression: implications for induction and inhibition of tumor angiogenesis. *Cancer Res* 1995; **55**: 4575–4580.
25 Gu WZ, Tahir SK, Wang YC, Zhang HC, Cherian SP, O'Connor S, *et al.* Effect of novel CAAX peptidomimetic farnesyltransferase inhibitor on angiogenesis *in vitro* and *in vivo*. *Eur J Cancer* 1999; **35**: 1394–1401.
26 Benjamin LE, Keshet E. Conditional switching of vascular endothelial growth factor (VEGF) expression in tumors: induction of endothelial cell shedding and regression of hemangioblastoma-like vessels by VEGF withdrawal. *Proc Natl Acad Sci USA* 1997; **94**:8761–8766.